

Multinuclear Solid-State NMR, DSC, and Conductivity Studies of Solid Polymer Electrolytes Based on Polyurethane/Poly(dimethylsiloxane) Segmented Copolymers

Chia-Liang Lin,[†] Hsien-Ming Kao,^{*,§} Ru-Rong Wu,[‡] and Ping-Lin Kuo^{*,†}

Department of Chemical Engineering, National Cheng Kung University, Tainan, Taiwan 701; Regional Instrumental Center, National Cheng Kung University, Tainan, Taiwan 701; and Department of Chemistry, National Central University, Chung-Li, Taiwan 32054

Received November 19, 2001

ABSTRACT: Solid polymer electrolytes based on polyurethane/poly(dimethylsiloxane) segmented copolymers (PS55) have been characterized by differential scanning calorimetry (DSC), ionic conductivity, and multinuclear solid-state NMR measurements. The results of DSC measurements indicate the formation of transient cross-links between Li⁺ ions and the ether oxygens on complexation with LiClO₄, resulting in an increase in the soft segment T_g . However, the soft segment T_g remains almost invariant at high salt concentration. There is a conductivity jump at around 310–330 K that the behavior of ionic conductivity changes from Arrhenius- to Vogel–Tamman–Fulcher (VTF)-type behavior. Below this jump temperature, the conductivity follows Arrhenius-like behavior, implying a diffusing mechanism for transport of the charge carriers where the charge carriers are decoupled from the segmental motion of the polymer chain. By contrast, the diffusion of charge carrier is assisted by the segmental motions of the polymer chains above the jump temperature, suggested by the VTF-like behavior. At high salt concentration, the ionic conductivity decreases due to the formation of ion pairs and/or ion clusters. Solid-state ¹³C NMR results from cross-polarization time constant (T_{CH}) measurements along with two-dimensional (2D) WISE NMR suggest that a significant decrease in the mobility of the soft segment as the salt is added. Polysiloxane backbone is not affected until at a higher salt concentration, as observed by the line width change in the ²⁹Si NMR spectrum. The onset temperature of ⁷Li motional line narrowing is correlated with the soft segment T_g . The activation energies obtained from ionic conductivity, ⁷Li line width, and T_1 measurements indicate that there is a strong correlation between the ionic conductivity of the solid polymer electrolyte and the mobile lithium cation.

Introduction

Since the discovery of ionic conductivity in some polyether-based polymer hosts complexed with alkali metal salts by Wright et al.^{1,2} in 1973, solid polymer electrolytes (SPEs) have received considerable attention with the increased request in performance. Because of the solvation power and complexing ability of poly(ethylene oxide) (PEO) to alkali metal ion, many studies on SPEs have dealt with the systems consisting of polyether-like structure with lithium salts. Recognizing that the ionic conductivity of PEO-based electrolytes is facilitated in the amorphous phase of PEO, significant research effort has been devoted in tailoring a polymer structure having a highly flexible backbone and a larger proportion of the amorphous phase. For instance, several comblike polymers,^{3–5} copolymers,⁶ and cross-linked polymers^{7,8} have been prepared, and their electric properties have been investigated. To prepare a solid polymer electrolyte for practical applications, the high conductivity and the good physical properties such as chemical stability and mechanical strength also have to be considered. Since polyether acts as polymer solvent favoring the transportation of ions, polysiloxane has a

high potential to be used as SPEs not only because of the existence of ether moiety inside it but also because of its chemical and thermal stability. When polysiloxane segments are introduced into the main chain of the comblike polymers,⁹ copolymers,¹⁰ and cross-linked polymers,¹¹ the obtained polymer electrolytes have high conductivity because of the flexibility of the polysiloxane segment. Furthermore, to improve the mechanical properties of SPEs for practical applications, linear segmented polyurethane might be a good choice.^{12–16} Because of their unique two-phase microstructure, the segmented polyurethanes find themselves very much useful as matrix materials for polymer electrolytes. The low glass transition temperature (T_g) and hence higher segmental motion of their soft segments leads to higher mobility of the dissolved ions and thus results in relatively high ionic conductivity. On the other hand, their hard segment domains can act as reinforcing fillers and hence contribute to the mechanical strength of the polymer electrolytes. Despite considerable interest in and effort devoted to SPEs, studies on the factors influencing the conductivity mechanism of the SPEs based on segmented polysiloxane modified polyurethane are still relatively limited.

Solid-state NMR has emerged as one of the highly sophisticated techniques to obtain the information about the ionic structure and mobility of the charge carriers and also to gain insight into the polymer–salt interactions in the polymer electrolytes.^{17–30} One important advantage of using NMR technique is its sensitivity to the dynamics of lithium ions and polymer chains based

[†] Department of Chemical Engineering, National Cheng Kung University.

[‡] Regional Instrumental Center, National Cheng Kung University.

[§] National Central University.

* Corresponding authors. Ping-Lin Kuo: Tel +886-6-2757575 ext 62658; Fax +886-6-2762331; e-mail plkuo@mail.ncku.edu.tw. Hsien-Ming Kao: Tel +886-3-4275054; Fax +886-3-4227664; e-mail hmkaio@cc.ncu.edu.tw.

dissolving the PS55 in DMAc with proper LiClO₄/DMAc solutions in various proportions to make polymer electrolytes with different amounts of LiClO₄. The mixed solution was cast onto aluminum plates, and the solvent was slowly removed under vacuum at 80 °C for 2 days. The films were then stored in a glovebox under an argon atmosphere (Vacuum Atmosphere Co.) for further measurements. The thickness of the films was controlled to be in the range 150–200 μm.

Solution NMR Experiments. High-resolution ¹H and ¹³C solution NMR experiments were performed on a Bruker AVANCE-300 spectrometer operating at resonance frequencies of 300.1 and 75.4 MHz for ¹H and ¹³C nuclei, respectively. The PS55 sample was dissolved in deuterated dimethyl sulfoxide (DMSO-*d*₆). The ¹H and ¹³C chemical shifts were referenced to tetramethylsilane (TMS) at 0.0 ppm.

DSC Thermograms. Thermal analysis of the polymer electrolytes was carried out on a DuPont TA2010 differential scanning calorimeter with a low-temperature measuring head and a liquid nitrogen-cooled heating element. In the first scan, a heating rate of 10 °C/min was used over the temperature range –150 to +150 °C. The second scan was performed after annealing the same sample used in the first scan at 150 °C for 10 min in order to remove the thermal history and then repeated the same procedure as that of first scan. Polymer electrolyte films were sealed in aluminum capsules and transferred out of the glovebox to perform thermal analysis. Glass transition temperatures (*T*_g) were reported as the midpoint of the transition process. All the thermograms were baseline corrected and calibrated against indium metal.

AC Impedance Measurements. Ac impedance measurements of the polymer electrolytes were performed using a CH Instrument model 604A electrochemical analyzer over a frequency range of 10 Hz–100 kHz with an amplitude of 10 mV. All the specimens were sandwiched by two polished stainless steel (SS304) blocking electrodes, and the cells were sealed with O-rings for conductivity tests. The conductivity values (σ) have been calculated from the equation $\sigma = (1/R_b)(t/A)$, where *R*_b is the bulk electrolyte resistance, *t* is the thickness, and *A* is the area of the sample.

Solid-State NMR Measurements. All the solid-state NMR experiments were performed on a Bruker AVANCE-400 spectrometer, equipped with a Bruker double-tuned 7 mm probe. The Larmor frequencies for ¹H, ⁷Li, ¹³C, and ²⁹Si nuclei are respectively 400.13, 155.45, 100.58, and 59.60 MHz. Magic angle spinning (MAS) of the samples in the range of 3–5 kHz was employed for obtaining ¹H, ¹³C, and ²⁹Si spectra and some ⁷Li spectra. The Hartmann–Hahn condition for ¹H → ¹³C cross-polarization (CP) experiments was determined using adamantane. The $\pi/2$ pulse lengths for ¹H and ⁷Li were typically 4 and 6 μs, respectively. The ¹H and ¹³C chemical shifts were externally referenced to TMS. The ¹H → ¹³C CP/MAS NMR spectra were recorded as a function of contact time ranging from 20 μs to 20 ms. Solid-state ²⁹Si NMR measurements were performed in order to determine the structure of the polysiloxane backbone. The Hartmann–Hahn condition for ¹H → ²⁹Si CP was determined on a cubic octamer silicic acid trimethylsilyl ester (Q₈M₈) sample. The optimal contact time for CP was found to be 3 ms. ²⁹Si chemical shifts were also externally referenced to TMS. ⁷Li and ¹H MAS NMR measurements were performed as a function of temperature and salt concentration with the purpose of establishing relationships between the dynamic properties of the Li⁺ ion and the polymer chain. ⁷Li NMR spectra were acquired under static and MAS conditions with and without proton decoupling. The ¹H and ⁷Li line widths were taken to be the full width at half-height (fwhh) of the peaks and measured as a function of temperature from 223 to 473 K. ⁷Li spin–lattice times (*T*₁) were measured by inversion–recovery methods. ⁷Li chemical shifts were referenced to a solid LiCl sample.

Two-Dimensional (2D) ¹H–¹³C WISE Experiments. ¹H wide-line spectra were acquired with the use of the 2D WISE NMR pulse sequence developed by Schmidt-Rohr et al.³¹ The pulse sequence consists of a 90_x degree pulse on the protons, which flips the magnetization into the *xy* plane, followed by a *t*₁ evolution period. The proton magnetization evolves under

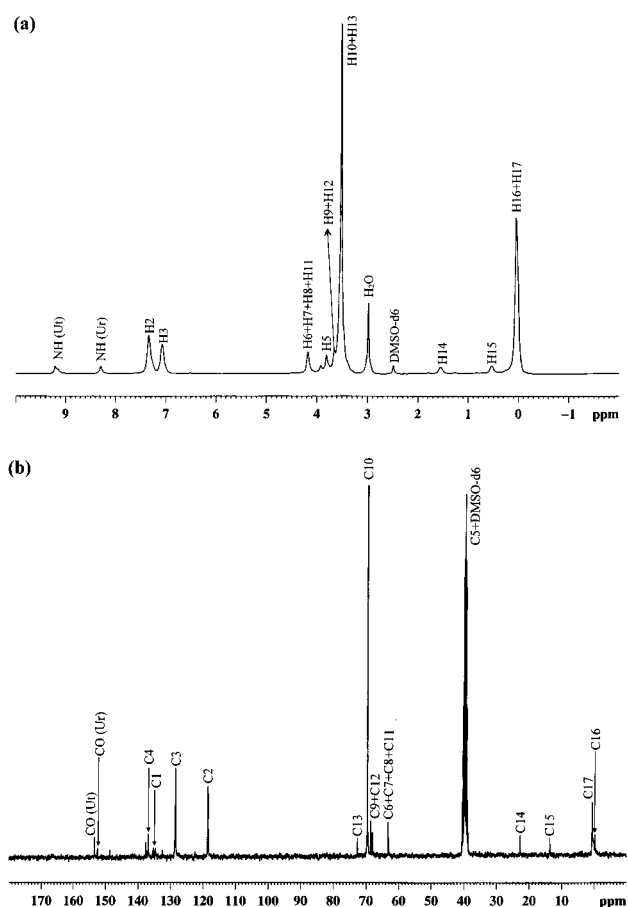


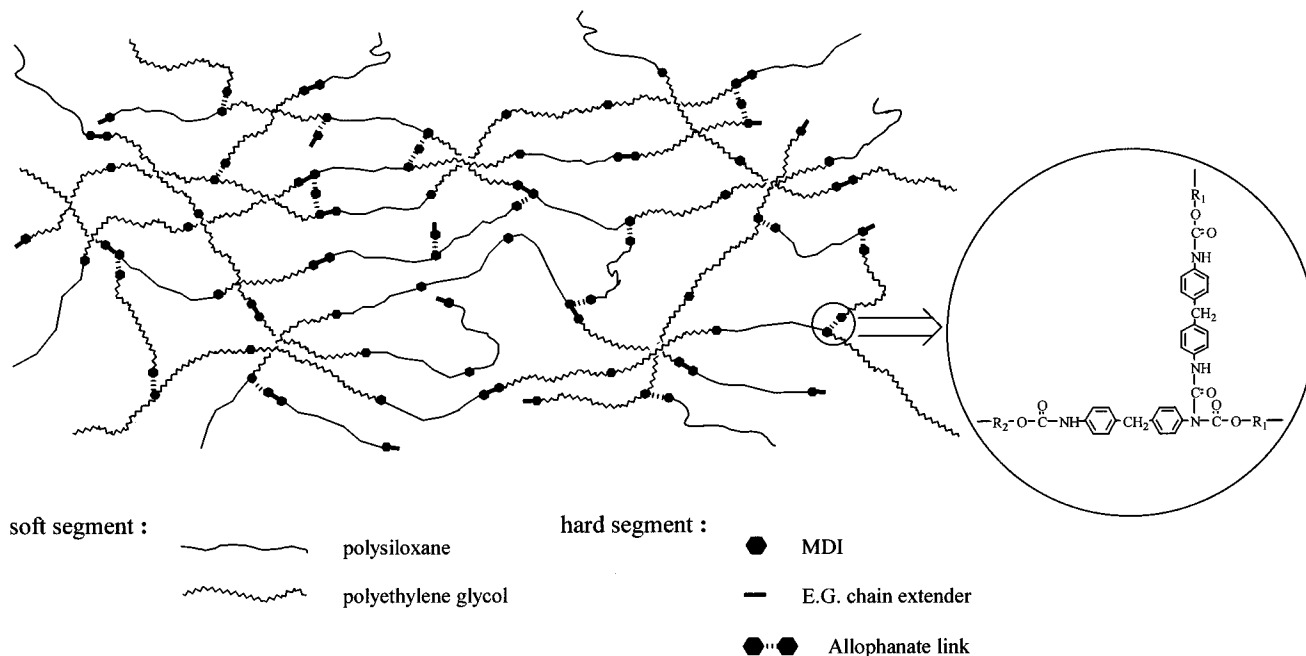
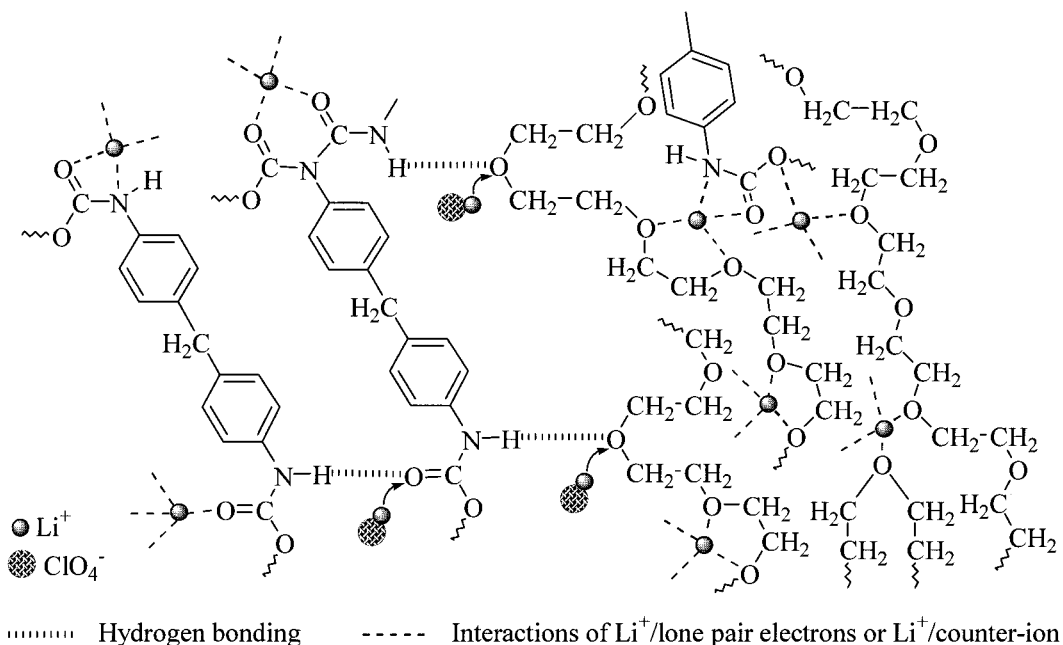
Figure 1. (a) ¹H and (b) ¹³C solution NMR spectra of PS55 copolymer.

the influence of dipolar coupling during the time *t*₁. Then a 90_{-x} degree pulse is applied to flip the magnetization back to the *z*-axis. In the simplest version of this experiment with the mixing time *t*_m = 0, the proton magnetization is transferred to the carbons by means of CP processes. The ¹³C signal is detected under MAS conditions during the time *t*₂. The experiment reveals proton wide-line spectra from the proton of polymer chains along the ω_1 dimension, resolved by the ¹³C chemical shifts of polymer chains along the ω_2 dimension. For each of these resolved ¹³C signals, a corresponding ¹H line can be obtained. Therefore, a correlation can be made between the chemical structure and segmental mobility of the polymer. Spectral widths of 40 and 333 kHz were used for the ω_2 and ω_1 dimensions, respectively. Typically 64 *t*₁ increments were used in the 2D WISE experiments. The CP and the dipolar decoupling field strengths were the same as those used for the ¹³C CP/MAS NMR experiments.

Results and Discussion

¹H and ¹³C Solution NMR: Identification of the Structure and Composition of PS55. ¹H and ¹³C solution NMR was used to identify the structure and to confirm the composition of the PS55 copolymer. The ¹H and ¹³C solution NMR spectra, acquired at 353 K due to low solubility at room temperature, of PS55 in DMSO-*d*₆ are shown in Figure 1. In the ¹H NMR spectrum (Figure 1a), the peaks at 9.21 and 8.29 ppm are assigned to urethane and urea protons, respectively, and the peaks at 7.34 and 7.07 ppm are assigned to the aromatic protons on MDI (H₂, H₃). The presence of urea groups at 8.29 ppm indicates that chain branching or cross-linking occurred due to the formation of allophanate links onto the main chain (inset structure, Scheme 2), which results from the additional reaction of the iso-

Scheme 2. Schematic Representation of PS55 Copolymer

Scheme 3. Schematic Representation of Coordination of Li^+ Ions in Different Domains of PS55

cyanate (MDI) with the urethane groups formed during the polymer formation.³² Methylene protons from EG and PEG are observed in the range 3.5–4.4 ppm. The presence of siloxane units in the polymer chain is confirmed by the appearance of the peak at 0.06 ppm, which is ascribed to the protons of methyl groups (H16, H17) attached on the silicon atom of siloxane units. The corresponding ^{13}C solution NMR spectrum is shown in Figure 1b. The actual PEG:MDI:FM-4411 mole ratio in the PS55 sample determined by ^1H solution NMR is 1.4:5.6:1, which is close to their theoretical ratio of 1:4:1.

DSC Thermograms. DSC was utilized to examine the effect of LiClO_4 on the morphologically based thermal transitions of the polyether soft segment T_g of PS55. As the hard and soft segments of PS55 are thermodynamically incompatible, separate thermal transitions are visible for both the hard and soft segments.

In polyether urethane, the soft segment T_g is observed in the negative temperature region where depending upon the amount of hard segment multiple thermal transitions are observed in the region of 70 °C to above 100 °C. Solvation of alkali metal salts by polymers has been reported to occur by means of coordination of the alkali metal cations with the ether oxygen of the polyethers. Many researchers^{12–16} have studied the effect of such coordination on the soft segment T_g . In PS55 polymer matrix, Li^+ ion could possibly coordinate in different domains (see Scheme 3), namely hard and soft domains. Thus, it is interesting to study the relationship between the morphology and the soft and hard segment T_g in PS55 polymer matrix.

Figure 2 displays the DSC thermograms obtained for PS55 electrolytes with various salt concentrations. The results of our thermal measurements are summarized

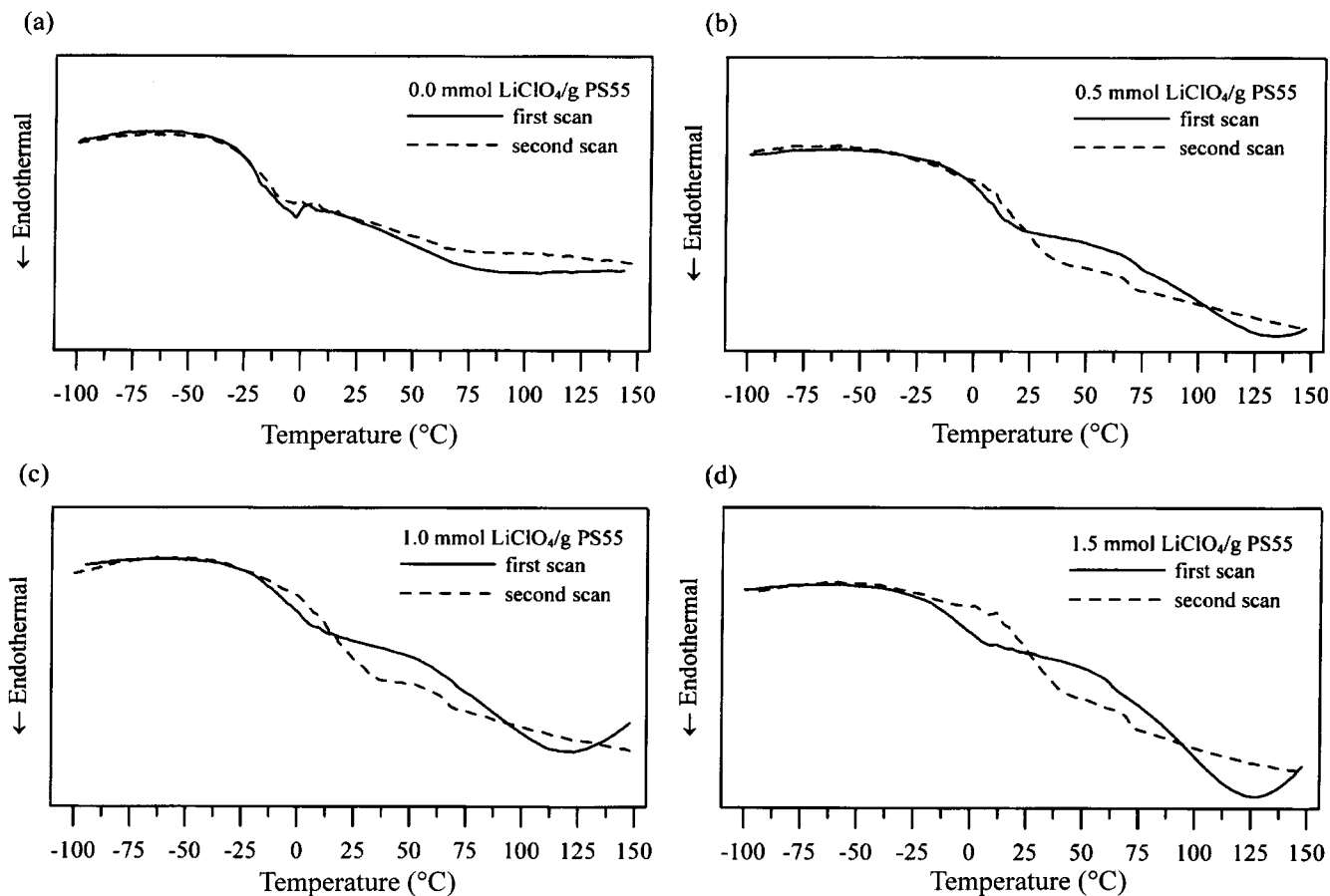


Figure 2. DSC results for LiClO_4 -doped PS55 samples.

Table 1. DSC Results for Lithium Salt Doped PS55

mmol $\text{LiClO}_4/\text{g PS55}$	first scan			second scan		ΔT_g (second scan – first scan)	
	T_{g1} (°C) ^a	T_{g2} (°C) ^b	T_{mc} (°C) ^c	T_{g1} (°C)	T_{g2} (°C)	ΔT_{g1}	ΔT_{g2}
0.0	-19.3			-20.5		-1.2	
0.2	-8.1		105.2	-2.2	68.1	5.9	
0.5	3.2	73.0	138.0	20.2	69.3	17.0	-3.7
1.0	-8.9	71.2	121.3	18.3	68.2	27.2	-3.0
1.5	-10.5	66.5	128.5	25.5	71.3	36.0	4.8
2.0	-7.3		134.6	36.5	74.0	43.8	

^a $T_{g1} = T_g$ of soft segment. ^b $T_{g2} = T_g$ of hard segment. ^c T_{mc} = the melting point of the crystalline PEG– LiClO_4 complex phase.

in Table 1. For the first scan, the glass transition temperature of soft segment (T_{g1}) is observed, but the glass transition temperature of hard segment (T_{g2}) is not obviously observed. However, the T_{g2} can be clearly observed in the second scan. In the first scan, the T_{g1} increases as the salt is added and reaches a maximum for 0.5 mmol $\text{LiClO}_4/\text{g PS55}$. This indicates that the solvation of the lithium cation with the PEG soft segment partially interrupts the local motion of the polymer segment via the formation of transient cross-links (see Scheme 3) and thus leads to an increase in the T_{g1} . As seen in Table 1, the T_{g1} , however, remains almost invariant at higher salt concentrations (>1.0 mmol/g). This may be attributed to the plasticizing effect due to the formation of ion pairs or ion clusters with increasing salt concentration.¹⁴ Ion pairs or ion clusters lose the ability to provide ionic cross-links, and hence a further increase in T_{g1} is not observed. The endothermic peaks appear in the range 105–150 °C for all doped samples. The endothermic peak can be ascribed to the melting temperature of the crystalline PEG– LiClO_4 complex phase. Both the plasticizing effect and the

crystalline PEG– LiClO_4 complex result in low ionic conductivity as shown below.

Annealing the samples at 150 °C for 10 min to remove the thermal history makes the microstructure initially observed by DSC (in the first scan) less complex, as shown as dashed lines in Figure 2. If the polymer matrix is in the amorphous state, then the thermal measurement results for the first and second scans at a fixed heating rate should be very similar, just like the thermal thermograms of undoped PS55 polymer matrix. It is of interest that the DSC thermograms in the second scan are dramatically different as compared to those in the first scan when the lithium salt is added. For the second scan, the endothermic peak due to the melting of the crystalline PEG– LiClO_4 complex disappears, and the glass transition of hard segment becomes evident from the DSC thermograms (see Figure 2). The absence of the melting peak for the crystalline complex phase in the second scan is probably due to the slow recrystallization of the complex phase that cannot be completed during the short cooling interval between the first and the second scan. The process of heat treatment (sample

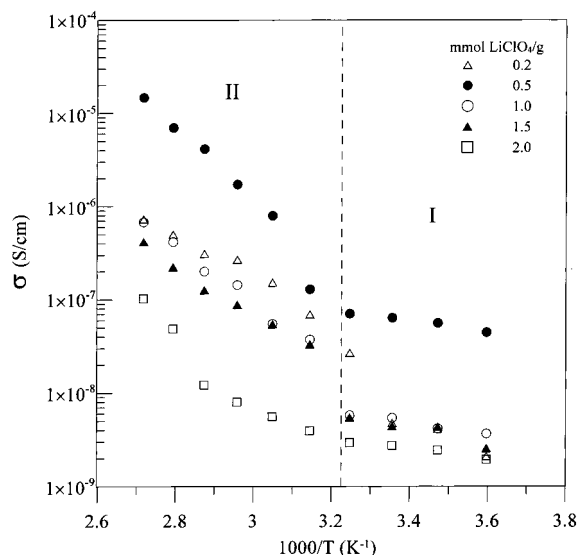


Figure 3. Temperature dependence of ionic conductivity of PS55 doped with different amounts of LiClO₄.

stayed isothermally at 150 °C and was then quenched to -150 °C) will involve the reorientation of polymer matrix that would result in a microphase separation between soft and hard segments; this is the reason that T_{g2} is more apparent in the second scan.

Another interesting phenomenon is that the soft segment T_g can be observed in the first and second scan. For instance, the T_{g1} in the second scan (18.3 °C) is considerably higher than that in first scan (-8.9 °C) for 1.0 mmol LiClO₄/g PS55. One possible explanation is that the crystalline PEG-LiClO₄ complex has been destroyed during heat treatment, and an increasing number of ether oxygens that can be coordinated to the Li⁺ cation make the PEG soft segment more stiff and therefore raise the soft segment T_{g1} in the second scan. Moreover, T_{g1} increases with increasing dopant amounts, indicating that there is no plasticizing effect observed in the second scan. This is due to the increasing number of ether oxygens in the polymer matrix is sufficient to avoid the formation of ion pairs or ion clusters. An increase in the T_{g1} with increasing lithium salt concentration can be attributed to the formation of transient cross-links. A similar trend has been observed for the glass transition temperature of hard segment, T_{g2} , in the second scan. Nevertheless, there is no significant change on T_{g2} as the salt concentration is increased. It implies that the coordination sites of hard segment might be preferentially formed and remain almost saturated irrelevant of salt concentration.

AC Impedance. Although ac conductivity of polyether polyurethane based polymer electrolyte systems has been reported earlier by many researchers,⁹⁻¹⁶ only few studies on the conductivity of SPEs based on segmented polysiloxane backbones were investigated.⁹⁻¹¹ Figure 3 shows the effect of LiClO₄ concentration and temperature on ionic conductivity of PS55 electrolytes. As shown in Figure 3, the conductivity increases in the lower salt concentration level and reaches a maximum for the 0.5 mmol LiClO₄/g PS55 sample. With further addition of salt, conductivity remarkably decreases, especially for the 2.0 mmol LiClO₄/g PS55 sample. It is generally accepted that ionic conductivity in polymer electrolytes is mainly attributed to a property of amorphous phase above their glass transition temperatures (T_g). The conductivity varies with a wide range of

factors, such as cation and anion types, salt concentration, temperature, etc. To design an effective SPEs, two opposite effects on the ionic transport properties must be thoroughly understood, namely the increase in the number of charge carriers and the decrease in free volume, which can be explained in the following way.

The conductivity of a homogeneous polymer electrolyte phase may be given as

$$\sigma(T) = \sum_i n_i q_i \mu_i \quad (1)$$

where n_i is the number of charge carriers of type i , q_i is the charge on each charge carrier, and μ_i is the mobility of charge carriers. The mobility is generally related to the diffusion coefficient, D_i , following the Nernst-Einstein equation:

$$\mu_i = (z_i e) D_i / k_B T \quad (2)$$

where k_B is the Boltzmann constant and $z_i e$ is the net electronic charge. As free volume theory proposed by Cohen and Turnbull³⁹ is applied to polymer electrolytes, it reveals that the average free volume of the polymer host is one of the determinants of ionic conductivity of the electrolytes. As the concentration of salt is increased, the number of charge carriers is also increased, but the average free volume is decreased as indicated from the increase in T_g owing to the interaction of Li⁺ with ether oxygens. The ion-transport process is correlated to the viscoelastic property of host polymer; i.e., the solvation of the lithium cation by the PEG soft segment partially interrupts the local motion of the polymer segment via the formation of transient cross-links and thus leads to an increase in the T_g . At low concentration of salt, the increase in the number of charge carriers dominates, and the decrease in free volume is compensated by the larger increase in the number of charge carriers. Hence, the conductivity is found to increase with salt concentration at the lower salt concentration level. When the salt concentration reaches 1.0 mmol LiClO₄/g PS55 or more, conductivity is decreased with increasing salt concentration. From Table 1, however, the soft segment T_g (T_{g1}) remains almost invariant at salt concentration levels higher than 1.0 mmol LiClO₄/g PS55 but lower than T_{g1} of 0.5 mmol LiClO₄/g PS55. It indicates that the number of effect charge carriers clearly dominates the conductivity in the PS55 electrolytes. Thus, it appears that the sudden drop in conductivity at higher salt concentrations is related to other factors such as the formation of ion pairs and/or ion clusters which tend to favor with increasing salt concentration. Owing to the low dielectric constant of polymer matrices, ion-ion interactions are equally important to polymer-ion interactions in polymer ionic conductors. At lower salt concentration level (below 0.5 mmol LiClO₄/g PS55), the transient cross-link density is low, and therefore the conductivity is controlled by the number of charge carriers. In this region, these are likely to be predominately free ions, and the ionic mobility is independent of salt concentration. In the ultraconcentrated medium, where the mean ionic separation is perhaps less than 0.5 nm, the strong ion-ion interactions must exist. Therefore, as the salt concentration increases, the less mobile ion pairs and clusters are predicted to form, acting as transient cross-linking species. Such ion cluster transient cross-linkings probably not only interrupt the interaction between lithium cation and oxygen

atom in soft segment but also increase the distance between the polymer chains. These effects can be used to explain why the soft segment T_g decreases as the salt concentration increases at high concentration range (above 1.0 mmol LiClO₄/g PS55). Ion pairs or ion clusters decrease the number density of the charge carriers present and also limit the mobility of the charge carriers throughout the polymer matrix. Therefore, the formation of ion pairs or ion clusters will result in a reduction in bulk conductivity.

Variation of conductivity with temperature for SPE's has been found to follow either the VTF (eq 3) or Arrhenius (eq 4) relationship, depending upon whether the ion mobility is coupled with the segmental motion of the polymer chains or not.

$$\sigma = AT^{-1/2} \exp\left(\frac{-\delta E_a}{k_B(T - T_0)}\right) \quad (3)$$

$$\sigma = A \exp\left(\frac{-E_a}{k_B T}\right) \quad (4)$$

where A is a constant proportional to the number of carrier ions, δE_a is the pseudoactivation energy related to polymer segmental motion, k_B is the Boltzmann constant, E_a is the activation energy, and T_0 is a reference temperature usually associated with the ideal T_g at which free volume disappears or the temperature at which the configurational entropy becomes zero. Application of VTF relationship for ion transport requires the coupling of the charge carriers with the segmental motion of the polymer chains.

As seen in Figure 3, it is clear that the temperature dependence of conductivity is not linear. The conductivity data do not fully follow the Arrhenius equation over all the investigated temperature ranges. All the conductivity curves of the studied samples exhibit two temperature regions, separated by a jump in temperature dependency. It is of interest to find that the conductivity of the complexes is less temperature dependent below 30 °C, but above this temperature the conductivity increases dramatically with increasing temperature. This behavior can be explained by a thermal dissociation of the ionic cross-links, which tend to relax from quadrupoles to ion pairs above 30 °C. Such a relaxation leads to an increased mobility of the ions and therefore increases the conductivity.⁴⁰ In the 0.5 mmol LiClO₄/g PS55 sample, for example, two separate temperature ranges, i.e., 270–310 K (region I), where the Arrhenius behavior is observed, and 310–370 K (region II), where the VTF equation is followed. A conductivity jump in the vicinity of 310 K is clearly observable. The results of activation energies from the slope of the curves in two separate temperature ranges as shown in Figure 3 are given in Table 2. The observed conductivity jump indicates a change in transport mechanism at this temperature. Above this temperature ionic motion is closely related to the polymer segment motion. The results of DSC evidence the absence of a first-order transition around 310 K, and thus a VTF equation is used to interpret the conductivity behavior observed in the region II. The conductivity of changing from Arrhenius behavior to VTF behavior is very different from that of traditional polyether-based electrolytes. From Table 2, it is important to notice that the activation energies obtained in the region II are significantly larger than those obtained in the region I. This

Table 2. Activation Energies Obtained from Conductivity Measurements^a

mmol LiClO ₄ /g PS55	E_a (I) (kJ/mol) ^b	δE_a (II) (kJ/mol) ^c
0.2		61.9
0.5	10.8	108.9
1.0	11.8	57.3
1.5	16.5	43.4
2.0	9.8	35.8

^a Note: The estimated accuracy is $\pm 10\%$. ^b In the temperature range of region I, the activation energies are calculated using eq 4. ^c In the temperature range of region II, the pseudoactivation energies δE_a at 328 K are calculated using eq 3 with T_0 to be about 50 K below the T_g of soft segments.

result is reasonable because the activation energy required for the glass transition process is expected to be larger than that for the diffusion process of Li⁺ cation. The 0.5 mmol LiClO₄/g PS55 sample exhibits highest activation energies in high-temperature regions, in line with its highest soft segment T_g value. The higher T_g can be expected to be due to lower segmental motions of the polymer chains and an accompanied higher activation energy. With further addition of salt, activation energies in both temperature regions gradually decrease with the increasing salt concentration. The obvious change in conductivity at high temperature of region II might be attributed to some factors such as the temperature region that is close to the hard segment T_g (about 70 °C) and/or the occurrence of aggregates at high temperature; both might affect the conductivity mechanism.

²⁹Si CP/MAS NMR. Solid-state ²⁹Si NMR spectroscopy has been used to provide information on the polysiloxane frameworks, such as the various local environments of silicon atoms of the polysiloxane backbone and the attachment of pendant groups. In particular, many of the chemical moieties associated with siloxane subunits can be identified on the basis of their chemical shifts.⁴¹ The sufficiently uniform placement of monomer units is confirmed by narrow and symmetric line shape of ²⁹Si NMR signals. A signal with broadening and asymmetry would indicate heterogeneity and variability of local surroundings of monomer units. Thus, ²⁹Si NMR can be used to probe the proximity of Li cations and the moiety containing silicon atoms when the salt is added to form the polysiloxane-based electrolyte.

As illustrated in Scheme 1, the considered polysiloxane materials are generally composed of two basic structure units, i.e., di- and mono-oxygen-substituted methylsiloxanes, represented by $-\text{Si}^*(\text{CH}_3)_2(\text{OSi})_2-$ (D type) and $-\text{Si}^*(\text{CH}_3)_2(\text{OSi})\text{CH}_2-$ (M type) structural units. The ²⁹Si CP/MAS NMR spectra of the PS55 sample doped with various amounts of LiClO₄ are shown in Figure 4. At -22 ppm a strong signal shows the resonance of the polysiloxane backbone, corresponding to the di-oxygen-substituted dimethylsiloxanes (D type). The shoulder at -21 ppm is due to the end-linked network of D-type structural units (DDM subunit). On the other hand, the resonance at 8 ppm can be assigned to mono-oxygen-substituted dimethylsiloxanes (M type). Although the D and M subunits are both difunctional in terms of network functionality, they appear in distinct regions of the chemical shifts because the number of oxygen bonded to silicon is the major determinant of the chemical shift. As seen in Figure 4, the presence of LiClO₄ does not disturb the chemical shift and line width of the peak at -22 ppm, indicating that there is

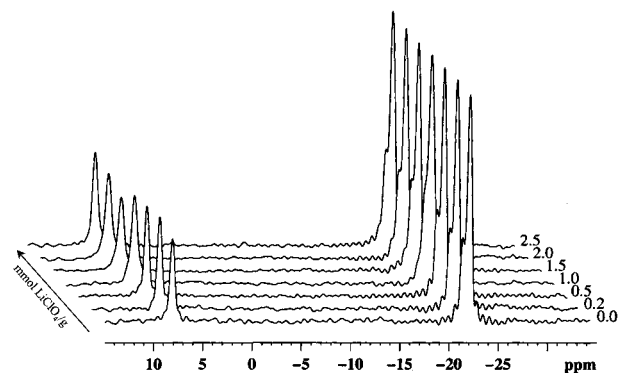


Figure 4. ^{29}Si CP/MAS spectra of PS55 doped with various amounts of LiClO_4 .

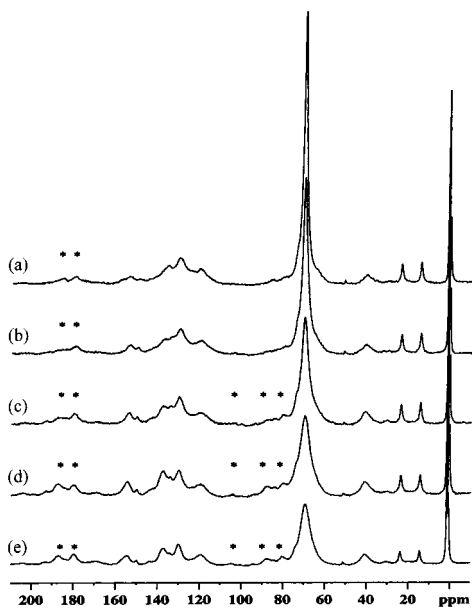


Figure 5. ^{13}C CP/MAS spectra of PS55 doped with (a) 0.0, (b) 0.2, (c) 0.5, (d) 1.0, and (e) 1.5 mmol of LiClO_4 . Asterisks denote spinning sidebands.

no significant interaction between the D-type Si subunit and the Li^+ cations. Presumably the steric effects caused by two methyl groups on the Si subunits limit the cation affinity to the ether oxygens of the Si subunits. Moreover, the decreased electron density on the oxygen atom due to $p-d$ π bonding between the oxygen and silicon atoms also does not favor the interaction. Although its line width does not alter at low salt concentration, the peak at 8 ppm becomes broadened at higher salt concentration. This indicates that a gradual interaction between the Li^+ cation and the ether oxygen atoms in the M-type Si subunits occurs at high concentration of Li salts, which can be used to correlated with the T_{CH} change of C15 as determined by variable contact time ^{13}C CP/MAS NMR measurements.

^{13}C CP/MAS NMR. Figure 5a shows the ^{13}C CP/MAS NMR spectrum, acquired at room temperature, of undoped PS55. Two peaks at 0.8 and 1.6 ppm for the methyl groups on the siloxane backbone are observed, indicating the methyl groups on the siloxane backbone are sensitive to the environments of the silicon atom. Two peaks centered at 148.5 and 154.6 ppm are observed in the carbonyl region and are assigned to the urethane and urea carbons, respectively. The urea units result from the branching or cross-linking as mentioned earlier (see Scheme 2). The peak at 70.8 ppm is assigned

Table 3. T_{CH} and $T_{1\rho}(\text{H})$ As Determined from Variable Contact Time ^{13}C CP/MAS NMR Experiments^a

carbon label	mmol LiClO_4 / g PS55	chemical shift (ppm)	T_{CH} (ms)	$T_{1\rho}(\text{H})$ (ms)
C17	0.0	1.6	2.74	132.10
	0.2	1.6	2.44	113.84
	1.0	1.6	1.76	50.55
C15	0.0	15.0	0.41	5.63
	0.2	14.7	0.35	7.13
	1.0	14.3	0.20	4.56
C14	0.0	24.1	0.33	6.25
	0.2	24.1	0.35	6.65
	1.0	24.4	0.14	4.62
C9, C10, C12	0.0	70.8	0.24	3.16
	0.2	70.8	0.15	2.02
	1.0	69.5	0.05	1.48

^a The estimated accuracy is $\pm 10\%$.

to those methylene carbons adjacent to ether oxygen (C9, C10, and C12). The small peaks at ca. 74 and 65 ppm are ascribed to the $-\text{OCH}_2$ groups that are adjacent to urethane (C6, C7, C8, and C11) and close to the siloxane segments (C13), respectively.

^{13}C CP/MAS NMR spectra were carried out at different LiClO_4 concentrations in order to analyze the effect of the amount of ionic salt on the polymeric chain and to study the chemical process involved. For comparison, Figure 5b–e displays the ^{13}C CP/MAS NMR spectra of the PS55 doped with various amounts of LiClO_4 . Upon addition of salt, significant line broadening is observed with the peak at 70.8 ppm. For example, the full width at half-height (fwhh) of the peak at 70.8 ppm is 210 Hz without the dopant, gradually increases with the increasing salt concentration, and becomes 580 Hz for 1.0 mmol LiClO_4 /g PS55 sample. This broadening indicates that the presence of Li salts causes a more broad distribution of the soft-segment environments and/or reduces the segmental motion of the polymer chains; the latter results from the electronic interaction between the Li^+ cations and the ether oxygen atoms in the soft segments. Thus, a broader peak is observed when the dopant exists. Similar behavior has been observed in ionic conducting polymers.⁴² The interaction between the lithium ion and the polymer chain is further supported by the change of its chemical shift with salt concentration. The chemical shift at 70.8 ppm for undoped PS55 gradually shifts upfield with increasing salt concentration, for example, shifts to 69.5 ppm for 1.0 mmol LiClO_4 /g PS55 sample (Figure 5d) by addition of LiClO_4 . The ^{13}C chemical shift change is also due to the interactions of the Li^+ cation with the polymer chains. Such upfield ^{13}C chemical shifts have been correlated to oxygen–cation interactions for poly(ethylene oxide) (PEO) and crown ether salt complexes.^{43,44} Hence, the increased line width and the upfield chemical shift of the peak at 70.8 ppm observed in the present system with increasing salt concentration indicates significant polymer–cation interactions. For more concentrated Li salt, there is no further significant changes in the chemical shifts and line widths for the peak at 70.8 ppm. As seen in Figure 5, it is interesting to note that the chemical shift of CH_2 groups (C15) adjacent to the siloxane backbone shows a gradual upfield shift with increasing salt concentration (see Table 3), suggesting that there are interactions between Li^+ ions and siloxane backbone at high salt concentration. As mentioned earlier, such interaction has been confirmed by the change of line width of M-type Si subunits in the ^{29}Si NMR spectrum. Another changes in the ^{13}C MAS NMR

spectra for doped samples appear in the aromatic regions. The broad peak at 135.8 ppm splits into two peaks corresponding to C1 and C4.

To gain more insight into the influence of Li⁺ ions on the polymer chain dynamics, ¹³C CP/MAS NMR experiments have been performed as a function of contact time, ranging from 20 μs to 20 ms. The T_{CH} and $T_{1\rho}^H$ measurements were obtained by fitting the CP signal intensities with the following formula:⁴⁵

$$M(t) = M_0 \exp(-t/T_{1\rho}^H)(1 - \exp(-t/T_{CH})) \quad (5)$$

where $M(t)$ is the peak intensity as a function of contact time t , M_0 is the normalization constant, $T_{1\rho}^H$ is the proton spin–lattice relaxation in the rotating frame, and T_{CH} is the cross-polarization time constant. The results of the contact time measurements for the selected carbons are presented in Table 3.

Since cross-polarization is a measure of the efficiency of magnetization transfer by the dipolar coupling from ¹H to ¹³C, the relative peak intensities for individual carbon groups as a function of contact time reflect both the magnitude of the dipolar coupling and motions of the C–H vector. CP time constant (T_{CH}) derived from variable contact time measurements can give quantitative descriptions of cross-polarization and relaxation behavior. Since cross-polarization is most efficient for the static ¹³C–¹H dipolar interactions, the less mobile carbon groups exhibit the faster cross-polarization rate or the shorter T_{CH} . Without adding the Li salts, the CH₂ groups (70.8 ppm) in the soft segments exhibit a T_{CH} value of 0.24 ms whereas the CH₂ group in the hard segment (C5, 40.0 ppm) exhibits a T_{CH} value of 0.02 ms. The slower growth in spin magnetization for the soft-segment peaks at 70.8 ppm, compared with that of the hard-segment peak at 40.0 ppm (all have two protons attached), is consistent with the higher mobility of the soft-phase carbons. This reflects that the rapid motion of the soft-segment carbons makes the CP signal transfer from the proton spins less efficient than for the hard-segment carbons. As seen in Table 3, there is a gradual decrease in T_{CH} for the peak at 70.8 ppm as the salt concentration is increased. The significant decrease in T_{CH} for the peak at 70.8 ppm with addition of salt suggests a possible coordination of Li⁺ ions with the ether oxygen atoms of the polymer chain, thereby restricting the segmental motion of soft segments. It is also noted that the T_{CH} 's for the carbon C14 and C15 in the siloxane segment remain nearly unaltered at low salt concentration whereas a decrease in their T_{CH} values is observed at high salt concentration (e.g., 1.0 mmol LiClO₄/g PS55).

As evident from Table 3, it is also clear that there are distinct protons spin reservoirs coupled to the different carbons, suggesting proton spin diffusion is relatively slow due to the phase separation in PS55. The $T_{1\rho}^H$ value for the protons associated with the soft segment suddenly drops upon addition of salt, reflecting that proton–proton spin diffusion become more efficient due to increased proton–proton dipolar interaction that results from an decrease in the segmental mobility. This observation indicates that the coordination between Li and the soft segments in the polymer chains effectively reduces the chain motion, resulting in the increase in the chain rigidity, and therefore increases proton–proton dipolar interaction. Both ¹³C chemical shifts and line widths indicate that ether carbons closest to the

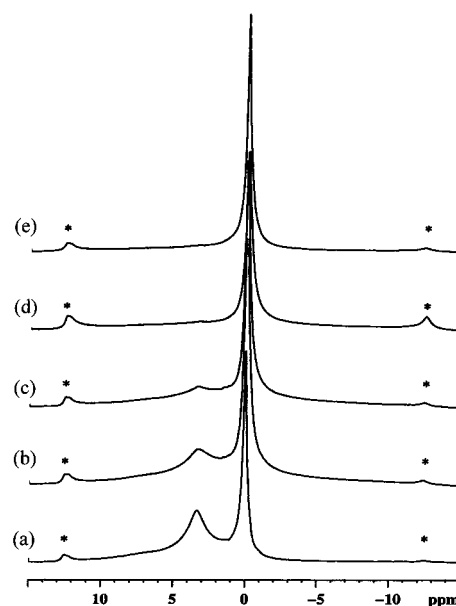


Figure 6. ¹H one-pulse NMR spectra of PS55 doped with (a) 0.0, (b) 0.2, (c) 0.5, (d) 1.0, and (e) 1.5 mmol of LiClO₄. Asterisks denote spinning sidebands.

siloxane backbone are not involved in coordination of the lithium cations unless the salt concentration is higher than 1.0 mmol LiClO₄/g PS55.

¹H MAS NMR. The ¹H MAS NMR spectra of PS55, acquired at room temperature, doped with different amounts of Li salts are shown in Figure 6. In the ¹H MAS NMR spectrum of undoped PS55 sample, a relatively broad peak of methylene protons adjacent to the ether oxygen atom (3.3 ppm) and a narrow peak of the methyl groups in the siloxane (0.0 ppm) are dominant. An increase in peak line width is observed as the salt concentration is increased. As evidenced in Figure 6, the intensity of the resonance at 3.3 ppm gradually decreases with increasing salt concentration and finally becomes barely visible at higher salt concentration because of an increasing dipolar interaction resulting in significant peak broadening. The increased dipolar interaction might result from the complexation of Li cations with the ether oxygen atoms in the polymer chain, which largely reduces the mobility of the polymer chain and thus increases both ¹H–¹H and ¹H–⁷Li dipolar interactions; the former interaction is more important than the latter. A long tail appears in the lower field (in the range of 6–8 ppm) is due to the protons in the aromatic ring, which is broadened because of strong ¹H–¹H dipolar coupling. A broad bump centered at ca. 2.0 ppm is ascribed to the other CH₂ groups that are not directly adjacently bonded to the ether oxygen. The marked difference in line width between the undoped and doped samples caused by the increased ¹H–¹H dipolar interactions, indicating that the mobility of the polymer chain is affected by addition of salts.

2D ¹H–¹³C WISE NMR. 2D WISE NMR has been widely used for determining dynamic heterogeneities in solid polymers.⁴⁶ As we can see from above, because of the limited chemical shift range for ¹H, one-dimensional ¹H NMR measurement alone is insufficient to distinguish the proton signals in different chemical environments in the solid state. In the 2D WISE NMR experiment, the high-resolution ¹³C CP/MAS NMR spectrum is displayed along one dimension, and the proton line

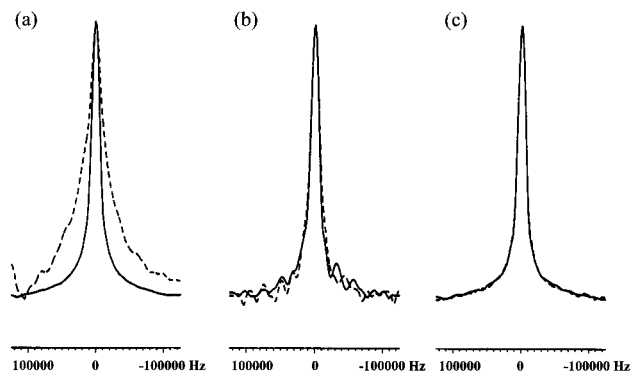


Figure 7. Projections of ^1H dimension of the 2D ^1H - ^{13}C WISE spectra associated with the selected carbons (a) 70.8 ppm, (b) 15.0 ppm, and (c) 1.6 ppm for undoped PS55 (solid lines) and PS55 doped with 1.0 mmol of LiClO_4 (dashed lines).

width associated with individual carbon sites is along the second dimension. By means of 2D WISE NMR, the spectroscopic information about the dynamic behavior within a system, reflected in the ^1H one pulse experiments, can be qualitatively assessed by examining the proton line shapes those are directly related to structural elements resolved in the ^{13}C CP/MAS NMR spectrum. Therefore, 2D WISE NMR spectroscopy is used here to further quantify chain mobility in order to confirm the results obtained from the CP time constant T_{CH} measurements. Moreover, the proton line widths obtained from our 2D WISE NMR measurements can be directly compared with other published results from different systems. Therefore, a deeper insight into the effect of addition of salt on the chain mobility associated with a specific segment can be revealed.

For convenience to make a comparison, Figure 7 shows the projections of ^1H dimension of the 2D ^1H \rightarrow ^{13}C WISE spectra, measured without the mixing time, associated with the selected carbons for undoped PS55 and 1.0 mmol LiClO_4/g PS55 samples, respectively. The line width of the ^1H line reflects the nature of the dipolar interaction between the protons and thus can be used to monitor the mobility of polymer chains. For the undoped PS55, all the selected carbons (1.6, 15.0, and 70.8 ppm) exhibit the same line width of 15.6 kHz (fwhh) in the ^1H dimension. The relatively narrow proton line width of 15.6 kHz at fwhh from the 2D WISE NMR revealed considerable chain mobility in comparison to most crystalline or semicrystalline polymers, which always exhibit proton line width larger than 50 kHz. Upon addition of salt to 1.0 mmol LiClO_4/g PS55, however, the line width of the ^1H line associated with resonance at 70.8 ppm increases from 15.6 to 37.1 kHz, while the line widths of the resonances at 1.6 and 15.0 ppm do not change at this salt concentration. This reflects a significant dynamic change along the soft segment in the polymer. Thus, the 2D WISE spectra further confirms our earlier conclusion that the mobility of the polymer chains decreases as the salt is added due to complexation of Li cations with the ether oxygen atoms.

^7Li NMR. Parts a and b of Figure 8 show the ^7Li static NMR spectra of a PS55 sample doped with 1.5 mmol LiClO_4/g PS55, acquired at 223 K without and with high-power proton decoupling, respectively. The spectrum of a spin $3/2$ (e.g., ^7Li) system in a powdered crystalline sample is expected to consist of a narrow component due to the $1/2 \leftrightarrow -1/2$ transition and a Pake doublet due to the $3/2 \leftrightarrow 1/2$ and $-1/2 \leftrightarrow -3/2$ satellite

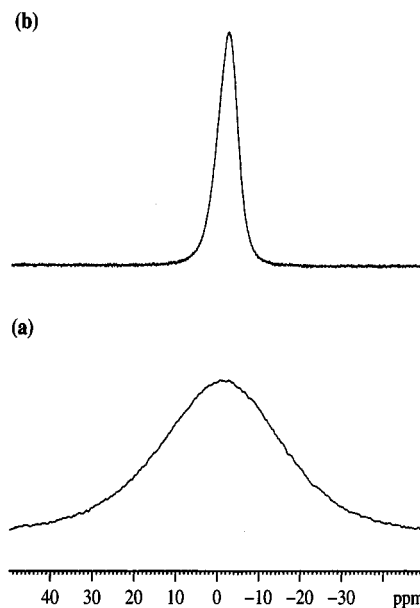


Figure 8. ^7Li static NMR spectra of a PS55 sample doped with 1.5 mmol LiClO_4/g PS55, acquired at 223 K without and with high-power proton decoupling.

transitions.⁴⁷ Inspection of the spectra at different temperatures shows that the line shape consists of only a relatively broad line. Since the PS55 polymer is a heterogeneous system, the absence of the satellite quadrupole powder pattern could be due to a wide distribution of possible electronic field gradients which results in an almost unobservable Gaussian-broadened line shape for the satellite transitions at temperatures below the glass temperature. Above the glass temperature, on the other hand, the weak and broad line associated with the quadrupolar satellite peaks is averaged out as the temperature is raised from T_g . Despite well-resolved first-order quadrupole satellite lines having been already observed in SPEs utilizing the same procedure used in this study, the quadrupole satellite lines are almost unobservable for the PS55-based electrolytes. For this reason, only the ^7Li central transition was analyzed in this study.⁴⁷

A significant reduction in the ^7Li line width (from 5.5 to 0.9 kHz) was achieved by the use of the decoupling techniques, which effectively removes the ^1H - ^7Li dipolar interactions of lithium cation and polymer backbone. Moreover, the line associated with the central transition is not broadened (up to first order) by the ^7Li quadrupole coupling. The central line broadening due to the second-order quadrupole interactions is expected to be small since its estimated contribution,⁴⁷ ν_Q^2/ν_L , is on the order of hertz. Therefore, the ^1H - ^7Li dipolar interaction is predominately responsible for the temperature behavior of the ^7Li line width. We can try to obtain information on the nuclear interactions by analyzing the second moment (M_2) of the NMR signal. While in crystals M_2 can be easily obtained by the Van Vleck formalism,⁴⁷ in the case of amorphous phases an experimental estimate of the second moment can be obtained by the relationship⁴⁸

$$M_2 = 0.721(^{1/2}\Delta H_{1/2})^2 \quad (6)$$

where $\Delta H_{1/2}$ is the fwhh expressed in gauss. According to eq 6, it follows that a value of $\sim 1.7 \text{ G}^2$ for ^7Li second moment can be obtained for all the studied samples.

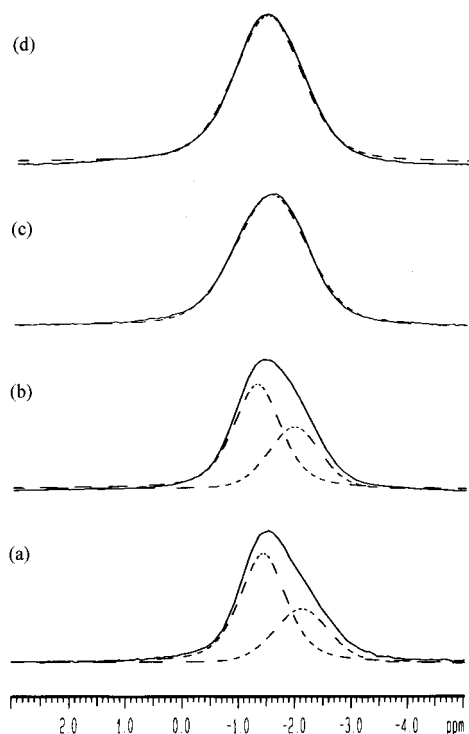


Figure 9. ^7Li MAS NMR spectra of PS55 doped with (a) 0.2, (b) 0.5, (c) 1.0, and (d) 1.5 mmol of LiClO_4 at 223 K at a spinning speed of 3 kHz, along with the deconvolution (dashed lines).

Besides the ^1H – ^7Li dipolar broadening of the ^7Li central line ($+1/2 \leftrightarrow -1/2$), there are other heteronuclear contributions from protons in the polymer chains and coupling with the chlorine and oxygen from ClO_4 species. Given the small gyromagnetic factors and/or low natural abundance of ^{13}C , ^{35}Cl , and ^{17}O stable isotopes, one can conclude that the residual line width of 0.9 kHz is mainly due to the ^7Li – ^7Li homonuclear interaction. Therefore, the ^7Li second moment contains the following dipolar contributions:

$$M_2(^7\text{Li}) = M_2(^7\text{Li}-^7\text{Li}) + M_2(^7\text{Li}-^1\text{H}) \quad (7)$$

Thus, the average ^7Li – ^7Li distance can be estimated following the Van Vleck expression⁴⁷ for the second moment, yielding ~ 4.5 Å, which is the same order of the average distance between two consecutive ether oxygen in the PEO chain (~ 3 Å) and also in good agreement with the findings of Wintersgill et al., who reported an average ^7Li – ^7Li separation of 4.7 Å in PVAc: $\text{LiClO}_4 = 8:1$.⁴⁹

To gather additional information regarding the Li ionic environment, high-resolution ^7Li MAS techniques were employed. The proton-decoupled ^7Li MAS NMR spectra as a function of salt concentration, recorded at 223 K, are displayed in Figure 9. For the 0.2 and 0.5 mmol LiClO_4/g PS55 samples (Figure 9a,b), the line shapes are asymmetric, and two components are directly visible, although they are only partially resolved, indicating two distinct lithium species with different local environments existing in the polymer structure. This implies that the microphase-separated structure of the polymer backbone can result in heterogeneous Li environments. These spectra could only satisfactorily be simulated on the basis of two components (site I (-1.4 ppm) and site II (-2.1 ppm)) with a site I:site II area ratio of approximately 0.65:0.35. This indicates that the

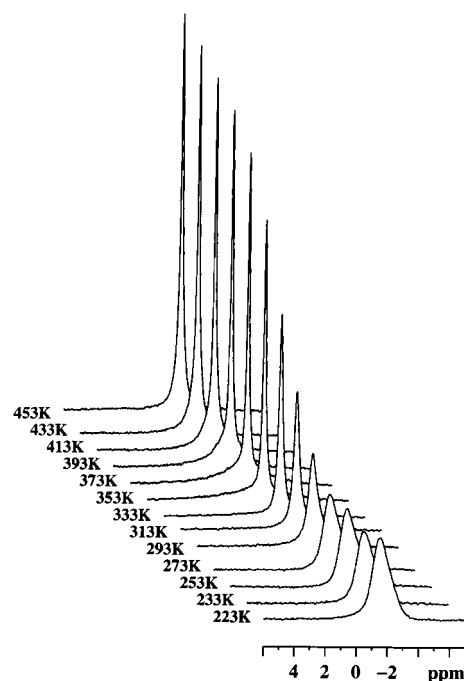


Figure 10. Temperature dependence of the ^7Li NMR spectra of PS55 doped with 0.2 mmol of LiClO_4 at temperatures as shown in the plot.

Li^+ cation is preferentially coordinated to site I. The intensity of site II increases slightly with an decrease in the intensity of site I when the salt concentration is increased from 0.2 to 0.5 mmol LiClO_4/g PS55, where the intensity of site I is normalized. Spinning sidebands are also observed at low temperatures, indicating that ^7Li quadrupolar interaction is increased due to the decrease in lithium mobility with decreasing the temperature. At high salt concentration (above 1.0 mmol LiClO_4/g PS55), on the other hand, the two sites are not resolved even at 223 K, and only a broad resonance is observed. In our previous study of $\text{LiClO}_4/\text{polyether poly(urethane urea)}$ electrolytes, we concluded that site II is attributable to the Li^+ cations coordinated to ether oxygen atoms in the soft segment, while site I is associated with urethane groups in the hard segment.⁵⁰ The above assignment is based on the results of conductivity measurements and the same ^7Li chemical shift as that of site II observed for electrolytes containing only soft segments. On raising the temperature to around 313–333 K (Figure 10), on the other hand, the asymmetric characteristic disappears, and the resulting peak is shifted toward site II. This result is significant in that it implies that at elevated temperatures corresponding to the conductivity jump region, where Li^+ ion transport readily occurs.

^7Li Line Width Measurements. Cation mobility in polymer electrolytes has previously been investigated by measuring the line width of solid-state ^7Li NMR spectra.⁵¹ At the lowest temperatures, the line widths are very broad and are approaching the rigid lattice line width. These broad line widths imply that the lithium ions are essentially immobile, and therefore the line width observed is the result of increased quadrupolar or internuclear dipole–dipole interactions. As the temperature increases, the line width decreases as a result of increased lithium ion mobility and hence averaging of these interactions.

The ^7Li line width measurement as a function of temperature for the $\text{LiClO}_4/\text{PS55}$ with various composi-

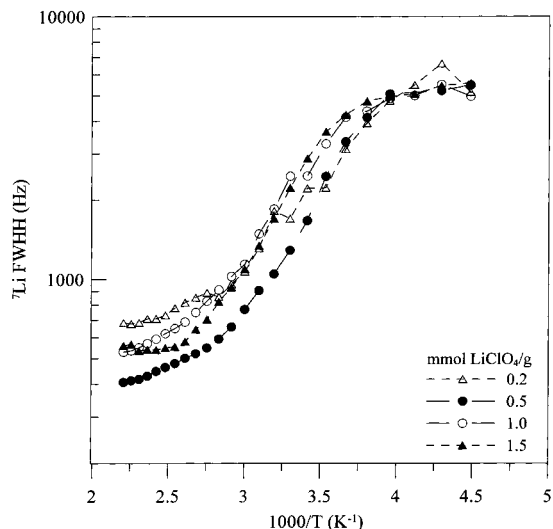


Figure 11. Line widths of ^7Li static NMR spectra of PS55 doped with various salt concentrations as a function of temperature.

tions is shown in Figure 11. As shown in Figure 11, the line width evolution with temperature can be described by a curve composed of two plateaus separated by a temperature range where rapid change in line width occurs. At low temperatures (<270 K), below the soft segment T_g of the systems, the line widths are broad. This suggests that the lithium ions are not mobile and thus are not conductive as evidenced from conductivity measurements. Upon increasing the temperature, the line widths are motionally narrowed, with the onset of narrowing correlating with the soft segment T_g . The lithium ions are therefore mobile near the DSC T_g , which is consistent with the NMR behavior observed in traditional polyether-based polymer electrolytes, which only show motional narrowing of the ^7Li line width once the soft segment T_g is exceeded. This implies that the mobility of cations appears to be closely associated with the segmental motions of the polymer above the glass temperature of soft segment. This phenomenon is corroborated by the sudden increase in conductivity above this temperature. In addition, the ^7Li line width for 0.5 mmol LiClO_4/g PS55 is smaller as compared to the other studied samples over the temperature range investigated (Figure 11), suggesting its higher cation mobility that correlates with its higher conductivity.

The motional narrowing of the ^7Li NMR line takes place when the rate of fluctuation of the local dipolar fields or the electric field gradient (EFG), which is generally described by a correction time, τ_c , is of the order of the rigid lattice line width, Δ_{RL}

$$1/\tau_c \approx \Delta_{\text{RL}} \quad (8)$$

An estimation of the activation energy for the narrowing process, $E_{\text{a,n}}$, may be obtained by the relationship⁴⁷

$$\tau_c = \frac{\alpha}{\Delta_{\text{HT}}} \tan \left[\frac{\pi}{2} \left(\frac{\Delta_{\text{HT}}}{\Delta_{\text{RL}}} \right)^2 \right] \quad (9)$$

where Δ_{HT} and Δ_{RL} are the fwhh's at a given temperature and in the rigid lattice, respectively, and α is a constant of the order of unity. Assuming that τ_c is

Table 4. Activation Energies Obtained from ^7Li Line Width and T_1 Measurements^a

mmol LiClO_4/g PS55	$E_{\text{a}}(\text{NMR})/\text{kJ mol}^{-1}$, line width ^b	$E_{\text{a}}(\text{NMR})/\text{kJ mol}^{-1}$, T_1
0.2	13.4	6.3
0.5	18.1	12.3
1.0	17.4	12.2
1.5	19.4	11.3

^a Note: The estimated accuracy is $\pm 10\%$. ^b The line width was measured from the whole peak envelope although there are two lithium sites existing at low salt concentrations at low temperatures.

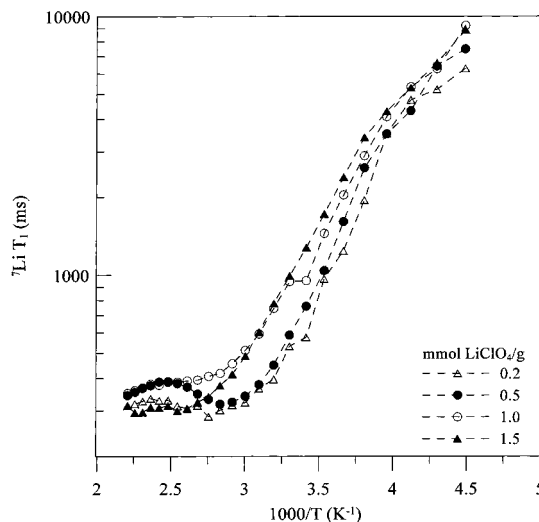


Figure 12. ^7Li T_1 measurements of PS55 doped with various salt concentrations as a function of temperature.

thermally activated

$$\tau_c = \tau_0 \exp(E_{\text{a,n}}/kT) \quad (10)$$

The activation energies, $E_{\text{a,n}}$, obtained from ^7Li line width measurements by fitting eqs 9 and 10 are listed in Table 4.

^7Li T_1 Measurements. NMR relaxation time measurements provide insight into how local interactions fluctuate at frequencies that are efficient at causing the nuclei to relax but are of most utility when they can be related to the local motions. Relaxation rates ($1/T_1$) are sensitive to fluctuations in the local environment on a time scale comparable to the inverse of the NMR resonance frequency, i.e., nanoseconds. ^7Li spin-lattice time (T_1) measurements are performed to analyze the lithium ion transport behavior over the temperature range 223–443 K. In general, in the case of quadrupolar nucleus ^7Li ($I = 3/2$), the spin-lattice relaxation should be described by a superposition of two or more exponentials.⁴⁷ Because of the small quadrupole moment of ^7Li , however, deviations from a single-exponential function are often difficult to detect as was also found in the present study. For all samples and temperatures, the ^7Li T_1 data were calculated using only one exponential function.

The evolution of the spin-lattice relaxation time T_1 as a function of the sample temperature is shown in Figure 12. It is shown that below ca. 300 K T_1 increases drastically, suggesting that the lithium ions become less and less mobile. T_1 curves with broad T_1 minima around 360 K are observed for 0.2 and 0.5 mmol LiClO_4/g PS55 samples. The blurred minimum observed with the low-

temperature slope having a shallower gradient can be attributed to a distribution of correlation times, implying that the local environment (nearest neighbor) of the lithium ions is heterogeneous as demonstrated in the proton-decoupled ^7Li MAS spectrum as shown in Figure 9. A minimum occurs at $\omega\tau_c = 0.6158$, and thus for a fixed ω , it indicates the frequency of the ionic motion. One can compare the relative mobilities of the nuclei in samples of differing composition by comparing the temperature positions of the minima. The T_1 minima of samples appear to have a trend to shift to higher temperatures with increasing Li^+ ion concentration, indicating less mobile nuclei. This can be correlated with the decreased conductivity observed for these samples. No definitive conclusion on the symmetry of the T_1 curve can be made because temperatures above the T_1 minimum were not possible with the present apparatus. However, when the temperature is close to the melting point of crystalline PEG– LiClO_4 complex phase (around 400 K), it appears to be another T_1 minimum for 0.5 mmol LiClO_4/g PS55.

It should be mentioned that the analysis of dynamic data in multicomponent systems is awkward because it is difficult to unambiguously identify the species whose dynamics are probed by these measurements. An analysis of ^7Li T_1 data reveals that both lithium sites exhibit similar T_1 behavior. Hence, as a preliminary analysis, it is assumed that a single correlation time describes the random motion of a nucleus relative to its environment, as predicted by the Bloembergen, Purcell, and Pound (BPP) relaxation model,⁵² giving rise to the following spectral density function at the Larmor frequency ω :

$$J(\omega) = \tau_c / (1 + \omega^2\tau_c^2) \quad (11)$$

The ^7Li NMR relaxation in lithium salt polymer complexes are mainly governed by two mechanisms: (i) quadrupolar relaxation, $(T_1^{-1})_Q$, due to the interactions between the nuclear quadrupole moment (eQ) and the fluctuations of the surrounding electric field gradients (EFG) produced by the charge distribution at the site of the nucleus, and (ii) the dipolar relaxation $(T_1^{-1})_{\text{dip}}$, which are produced by the random fluctuation of the lithium homonuclear (^7Li – ^7Li) and heteronuclear (^7Li – ^1H) dipolar interactions:

$$T_1^{-1} = (T_1^{-1})_{\text{dip}} + (T_1^{-1})_Q \quad (12)$$

Treating the dipole–dipole interaction as a perturbation on the Zeeman interaction, one obtains the following expressions for the relaxation rates:⁴⁷

$$(T_1^{-1})_{\text{dip}} = C_1[J(\omega_I) + J(2\omega_I)] + C_2[J(\omega_I - \omega_S) + 3J(\omega_I) + 6J(\omega_I + \omega_S)] \quad (13)$$

where the first term on the right-hand side of eq 13 describes the interaction between like spins I–I (e.g., ^7Li – ^7Li) and the second term describes the interaction between unlike spins I–S (e.g., ^7Li – ^1H). The constants C_1 and C_2 depend on the particular spin interaction responsible for the relaxation. The temperature and frequency dependence of $(T_1^{-1})_Q$ is the same as that of the first term of eq 13, except for the fact that the proportionality constant are proportional to the square

of the nuclear quadrupole coupling constant, ν_Q :

$$(T_1^{-1})_Q = \frac{3\pi^2}{10} \frac{2I+3}{I^2(2I-1)} \left(1 + \frac{\eta^2}{3}\right) \nu_Q^2 [J(\omega) + 4J(2\omega)] \\ \approx \frac{2\pi^2}{5} \nu_Q^2 [J(\omega) + 4J(2\omega)] \quad (14)$$

The asymmetry parameter, η , of the EFG tensor varies from 0 to 1.

An estimate of the quadrupole coupling constant (ν_Q) can be obtained by using the ^7Li second moment to calculate the dipolar contribution to the spin–lattice relaxation at the rate maximum $(T_1^{-1})_{\text{dip}}$ and comparing the result with the experimental value in Figure 12, $(T_1^{-1})_{\text{max}} \approx 3.7 \text{ s}^{-1}$ for 0.5 mmol LiClO_4/g PS55 sample. An estimate of the lithium second moment, M_2 , can be obtained from the Gaussian shape of the central line at low temperature, yielding $M_2 \approx 1.7 \text{ G}^2$ for 0.5 mmol LiClO_4/g PS55 sample. Then, the dipolar contribution to the spin–lattice relaxation rate can be calculated from the lithium second moment, and the ^7Li – $\{^1\text{H}\}$ decoupling results. From eq 13 it follows that $(T_1^{-1})_{\text{dip}}$ is $\sim 0.2 \text{ s}^{-1}$ at the maximum relaxation rate ($(T_1^{-1})_{\text{max}} \approx 3.7 \text{ s}^{-1}$). According to eq 12, the magnitude of the quadrupole spin–lattice relaxation would be $(T_1^{-1})_Q \approx 3.5 \text{ s}^{-1}$. Therefore, the fluctuations of the quadrupolar interaction due to the Li^+ motions are mainly responsible for the spin–lattice relaxation of the ^7Li nuclei, consistent with the results reported by Steven.⁵¹ Thus, the ^7Li T_1 measurement provides a most convenient means to monitor the change of quadrupolar interaction, which revealed the lithium mobility and diffusion behavior. The value of $(T_1^{-1})_Q$ at the maximum rate is only dependent upon the strength of the quadrupolar interaction, described by the prefactors in eq 14. This gives a quadrupole coupling constant $\nu_Q \approx 30 \text{ kHz}$, which is of the same order of magnitude than those reported for SPEs.⁵¹

NMR relaxation is usually regarded as a thermally activated process that can be described by an activation energy. Table 4 lists the activation energies as determined from Figure 12, the values having been calculated from the low-temperature slopes of the relaxation curves. In the present data, it is difficult to estimate the activation energies from the high-temperature side. A kink was observed in the T_1 curve at around 260–270 K, close to the onset temperature as conductivity changed from Arrhenius to VTF behavior. This is significant not least because it connects the observed NMR behavior with the conductivity behavior of the samples. It is important to notice that the activation energies obtained from ^7Li line width measurements are sensibly larger than those obtained from ^7Li T_1 measurements (see Table 4). These results indicate that a single relaxation model BBP cannot be used along the whole temperature interval, although the curves can be adequately fitted with a single correlation time. Because of the heterogeneity of mobility in different sites of the PS55 polymer chain, another relaxation models should be used to understand this behavior, such as a distribution of correlation times (e.g., the Kohlrausch–Williams–Watts function)^{53,54} and/or a quasi-two-dimensional BBP.⁵⁵

Conclusions

The effect of changing salt concentration on the lithium cation environment and mobility in solid poly-

mer electrolytes based on polyurethane/polydimethylsiloxane segmented copolymer has been investigated. The conductivity behavior changed from Arrhenius- to VTF-type temperature dependence around 330 K, suggesting that charge-carrier diffusion is still assisted by segmental motion of the polymer in the high-temperature region although conductivity is decoupled from the polymer motions in the low-temperature region.

Multinuclear NMR studies have been performed to probe the specific interaction between polymer chain and Li^+ cation and the behavior of the mobile ionic species. These combined experiments point out that a strong correlation is observed between the behavior of the solid electrolyte and the mobile lithium species. As evident from ^{29}Si NMR, there is negligible interaction between siloxane backbone and lithium cation unless a large amount of salt is added.

Acknowledgment. Support from the National Science Council of Taiwan, Republic of China, is gratefully acknowledged.

References and Notes

- Fenton, B. E.; Parker, J. M.; Wright, P. V. *Polymer* **1973**, *14*, 589.
- Wright, P. V. *Br. Polym. J.* **1975**, *7*, 319.
- Tada, Y.; Sato, M.; Takeno, N.; Nakacho, Y.; Shigehara, K. *Chem. Mater.* **1994**, *6*, 27.
- Inoue, K.; Nishikawa, Y.; Tanigaki, T. *Macromolecules* **1991**, *24*, 3464.
- Blonsky, P. M.; Shriver, D. F.; Austin, P.; Allcock, H. R. *J. Am. Chem. Soc.* **1984**, *106*, 6854.
- Watanabe, M.; Rikukawa, M.; Sanui, K.; Ogata, N. *Macromolecules* **1986**, *19*, 188.
- Andrei, M.; Marchese, L.; Roggero, A.; Prosperi, P. *Solid State Ionics* **1994**, *72*, 140.
- Watanabe, M.; Nishimoto, A. *Solid State Ionics* **1995**, *79*, 306.
- Fish, D.; Khan, I. M.; Wu, E.; Smid, J. *Br. Polym. J.* **1988**, *20*, 281.
- Nagaoka, K.; Naruse, H.; Shinohara, I.; Watanabe, M. *J. Polym. Sci., Polym. Lett. Ed.* **1984**, *22*, 659.
- Ogumi, Z.; Uchimoto, Y.; Takehara, Z. *Solid State Ionics* **1989**, *35*, 417.
- Watanabe, M.; Sanui, K.; Ogata, N. *Macromolecules* **1986**, *19*, 815.
- Seki, M.; Sato, K. *Makromol. Chem.* **1992**, *193*, 2971.
- van Heumen, J. D.; Stevens, J. R. *Macromolecules* **1995**, *28*, 4268.
- Ferry, A.; Jacobsson, P.; van Heumen, J. D.; Stevens, J. R. *Polymer* **1996**, *37*, 737.
- Wen, T. C.; Wu, M. S.; Yang, C. H. *Macromolecules* **1999**, *32*, 2712.
- Kim, C. H.; Park, J. K.; Kim, W. J. *Solid State Ionics* **1999**, *116*, 53.
- Mustarelli, P.; Quartarone, E.; Capiglia, C.; Tomasi, C.; Magistris, A. *Solid State Ionics* **1999**, *122*, 285.
- Ali, F.; Forsyth, M.; Garcia, M. C.; Smith, M. E.; Strange, J. H. *Solid State Nucl. Magn. Reson.* **1995**, *5*, 217.
- Ward, I. M.; Boden, N.; Cruickshank, J.; Leng, S. A. *Electrochim. Acta* **1995**, *40*, 2071.
- Stallworth, P. E.; Greenbaum, S. G.; Croce, F.; Slane, S.; Salomon, M. *Electrochim. Acta* **1995**, *40*, 2137.
- Forsyth, M.; Meakin, P. M.; MacFarlane, D. R. *Electrochim. Acta* **1995**, *40*, 2339.
- Forsyth, M.; MacFarlane, D. R.; Meakin, P.; Smith, M. E.; Bastow, T. J. *Electrochim. Acta* **1995**, *40*, 2343.
- Forsyth, M.; Garcia, M.; MacFarlane, D. R.; Meakin, P.; Ng, S.; Smith, M. E. *Solid State Ionics* **1996**, *85*, 209.
- Shan, W.; Zax, D. B. *Electrochim. Acta* **1997**, *42*, 3513.
- Williamson, M. J.; Southall, J. P.; Hubbard, H. V. St. A.; Johnston, S. F.; Davies, G. R.; Ward, I. M. *Electrochim. Acta* **1998**, *43*, 1415.
- Ferry, A.; Oradd, G.; Jacobsson, P. *Electrochim. Acta* **1998**, *43*, 1471.
- Ng, S. T. C.; Forsyth, M.; MacFarlane, D. R.; Garcia, M.; Smith, M. E.; Strange, J. H. *Polymer* **1998**, *39*, 6261.
- Forsyth, M.; Jiazeng, S.; MacFarlane, D. R. *Electrochim. Acta* **2000**, *45*, 1237.
- Forsyth, M.; MacFarlane, D. R.; Hill, A. J. *Electrochim. Acta* **2000**, *45*, 1243.
- Schmidt-Rohr, K.; Clauss, J.; Spiess, H. W. *Macromolecules* **1992**, *25*, 3272.
- Hepburn, C. *Polyurethane Elastomers*, 2nd ed.; Elsevier: London, 1991; p 4.
- Luo, N.; Wang, D. N.; Ying, S. H. *Macromolecules* **1997**, *30*, 4405.
- Coleman, M. M.; Lee, K. H.; Skrovanek, D. J.; Painter, P. C. *Macromolecules* **1986**, *19*, 2149.
- Coleman, M. M.; Skrovanek, D. J.; Hu, J.; Painter, P. C. *Macromolecules* **1988**, *21*, 59.
- Lee, H. S.; Wang, Y. K.; Hsu, S. L. *Macromolecules* **1987**, *20*, 2089.
- Lu, X.; Weiss, R. A. *Macromolecules* **1991**, *24*, 4381.
- Wang, H. L.; Kao, H. M.; Digar, M.; Wen, T. C. *Macromolecules* **2001**, *34*, 529.
- Cohen, M. H.; Turnbull, D. *J. Chem. Phys.* **1959**, *31*, 1164.
- Hawker, C. J.; Chu, F.; Pomery, P. J.; Hill, D. J. T. *Macromolecules* **1996**, *29*, 3831.
- Beshah, K.; Mark, J. E.; Ackerman, J. L. *Macromolecules* **1986**, *19*, 2194.
- O'Gara, J. F.; Nazri, G.; MacArthur, K. M. *Solid State Ionics* **1991**, *47*, 87–96.
- (a) Ibemisi, J. A.; Kimsinger, J. B. *J. Polym. Sci., Polym. Chem. Ed.* **1980**, *18*, 1123–1126. (b) Bekturov, E. A.; Kudaibergenov, S. E.; Bakanova, Z. K.; Vshamov, V. Z.; Kanapyanova, G. S. *Polym. Commun.* **1985**, *26*, 81–83.
- (a) Popov, A. I.; Smitana, A. J.; Kintzinger, J.-P.; Nguyen, T. T. *Helv. Chim. Acta* **1980**, *63*, 668–673. (b) Fedarko, M.-C. *J. Magn. Reson.* **1973**, *12*, 30–35.
- Mehring, M. *Principles of High-Resolution NMR in Solids*, 2nd ed.; Springer-Verlag: New York, 1983.
- Schmidt-Rohr, K.; Spiess, H. W. *Multidimensional Solid-State NMR and Polymers*; Academic Press: New York, 1994.
- Abraham, A. *The Principles of Nuclear Magnetism*; Clarendon: Oxford, 1961.
- Poole, Ch. *Electron Spin Resonance*, 2nd ed.; Wiley: New York, 1983.
- Wintersgill, M. C.; Fontanella, J. J.; Calame, J. P.; Smith, M. K.; Jones, T. B.; Greenbaum, S. G.; Adamic, K. J.; Shetty, A. N.; Anden, C. G. *Solid State Ionics* **1986**, *18/19*, 326.
- Wang, H. L.; Kao, H. M.; Wen, T. C. *Macromolecules* **2000**, *33*, 6910.
- Chung, S. H.; Jeffrey, K. R.; Steven, J. R. *J. Chem. Phys.* **1991**, *94*, 1803.
- Bloembergen, N.; Purcell, E. M.; Pound, R. V. *Phys. Rev.* **1948**, *73*, 679.
- Williams, G. *J. Non-Cryst. Solids* **1991**, *131–133*, 1.
- Maring, D.; Meurer, B.; Weill, G. *J. Polym. Sci., Part B: Polym. Phys.* **1995**, *33*, 1235.
- Kuchler, W.; Heitjans, P.; Payer, A.; Schollhorn, R. *Solid State Ionics* **1994**, *70*, 434.

MA012012Q